frontiers | Frontiers in Earth Science

ORIGINAL RESEARCH
published: 29 June 2022
doi: 10.3389/feart.2022.919923

Genetic Mechanism of Pyrite in the Shale of the Longmaxi Formation and Its Influence on the Pore Structure: A Case Study of the Changning Area, South Sichuan Basin of SW China

Jiang He[1], Lan Yang[1], Xuewen Shi[2], Shengxian Zhao[2], Lieyan Cao[2], Shulin Pan[1], Feng Wu[1] and Meng Wang[3,4]**

[1]School of Geoscience and Technology, Southwest Petroleum University, Chengdu, China, [2]Shale gas Research Institute of PetroChina Southwest Oil and gas Field Company, Chengdu, China, [3]School of Chemistry and Chemical Engineering, Chongqing University of Science and Technology, Chongqing, China, [4]Key Laboratory of Shale Gas Exploration, Ministry of Natural Resources, Chongqing Institute of Geology and Mineral Resources, Chongqing, China

OPEN ACCESS

Edited by:
Wenlong Ding,
China University of Geosciences, China

Reviewed by:
Zhu Baiyu,
Yangtze University, China
Lei Liu,
Chengdu University of Technology, China

***Correspondence:**
Jiang He
hejiang_swpu@126.com
Meng Wang
wangmeng_cqust@126.com

Specialty section:
This article was submitted to Economic Geology, a section of the journal Frontiers in Earth Science

Received: 14 April 2022
Accepted: 23 May 2022
Published: 29 June 2022

Citation:
He J, Yang L, Shi X, Zhao S, Cao L, Pan S, Wu F and Wang M (2022) Genetic Mechanism of Pyrite in the Shale of the Longmaxi Formation and Its Influence on the Pore Structure: A Case Study of the Changning Area, South Sichuan Basin of SW China. Front. Earth Sci. 10:919923. doi: 10.3389/feart.2022.919923

Pyrite is a mineral that is commonly found in shale gas reservoirs. Its genetic mechanism and impact on pore and organic matter in shale gas reservoirs are critical for shale gas exploration. This study selects the Longmaxi shale (Lower Silurian) in the Changning area of the southern Sichuan Basin by comprehensively using a scanning electron microscope (SEM), X-ray diffraction (XRD), total organic carbon (TOC), and image processing technology. The type and characteristics of pyrite in shale reservoirs are studied, the sedimentary environment and genetic mechanism of pyrite are analyzed, and the influence of pyrite formation on organic matter enrichment and reservoir formation is evaluated. The results showed that pyrite in shale primarily forms framboidal pyrite, euhedral pyrite, and subhedral pyrite, with particle sizes ranging from 1 to 15 μm. The maximum framboid diameter (MFD) is less than 20 μm, with the average particle size distribution of 3–5 μm. These parameters indicate the vulcanization and blocking environment. The reducing environment promotes organic matter enrichment and preservation. Framboidal pyrite has two genetic sequences: rich organic matter and poor organic matter. The development of organic matter will limit the continuous radial growth of pyrite and is conducive to the protection of pores, and the formation of pyrite can reduce the activation energy of kerogen reaction and catalyze the hydrocarbon generation of organic matter, resulting in higher gas content. The framboidal pyrite content can be used to predict high-quality shale gas reservoirs.

Keywords: framboidal pyrite, shale gas reservoir, sedimentary environment, Longmaxi Formation, Sichuan Basin

1 INTRODUCTION

In recent years, there has been a growing interest in the mechanism of shale gas accumulation, migration, and storage, as well as the pore structure and sedimentary environment of the reservoir (Zou et al., 2011). As a characteristic mineral in an organic-rich shale formation, pyrite plays a positive role in shale gas development due to its structural characteristics, environmental significance, and impact on shale reservoirs and shale gas development (Han and Li, 2019).

Authigenic pyrite is the main product of sulfate reduction in an anoxic marine environment and widely occurs in marine sediments on the continental margin. The main factors controlling the formation of pyrite are the degradation of organic matter and the anaerobic oxidation of methane. Pyrite has mostly bedding distribution, lenticular structures, and some linear structures, but under the microscope, it has framboidal, massive, euhedral, nodular, and fissure filling shapes (Wilkin et al., 1996; Wei et al., 2016). Different forms indicate different formation processes, each representing a distinct formation environment, particularly framboidal pyrite, which can be classified as quasi syngenetic or diagenetic. The former occurs in sulfide water bodies, while the latter occurs in anoxic void water in sediments beneath oxidized or oxygen-depleted water bodies. They differ in shape, particle size, and sulfur isotope (Wei et al., 2016).

The surrounding environment limits the microcrystal of framboidal pyrite aggregate during its growth and its particle size change, which correlates well with the degree of hypoxia in the water body. It is a reliable index to distinguish the redox conditions of paleo-sedimentary water bodies (Wilkin et al., 1996; Wilkin and Barnes, 1997; Chang et al., 2009,2011; Wei et al., 2016), which has great significance in judging the sedimentary environment of shale reservoir. Chang and Chu (2011) and Zhou and Jiang (2009) refined the sedimentary environment into three oxidation levels, weak oxidation and sulfidic, using framboidal pyrite. Cui et al. (2013) proposed that pyrite has a positive impact on oil and gas reservoirs, hydrocarbon generation, and expulsion. Nie and Zhang (2012) concluded that pyrite plays a vital role in shale gas accumulation by studying the controlling factors of shale gas accumulation conditions. Cao et al. (2018) concluded that pyrite contributes to organic matter hydrocarbon generation and shale gas development by examining pyrite in different horizons in the Yangtze region and combined it with previous research results. Zhu et al. (2018) believed that pyrite can affect oil and gas accumulation in the reservoir and promote oil and gas accumulation and hydrocarbon generation and expulsion of organic matter.

The contribution of pyrite developed in shale to the pore system is now widely accepted (Li et al., 2019; Li et al., 2020; Liu et al., 2022), but there are still some disputes about its porosity development degree and the importance of pores related to pyrite. The contribution of pore development characteristics related to the pyrite of a shale reservoir cannot be quantified (Fan et al., 2020). From the perspective of diagenesis, pyrite cementation will occupy a portion of the primary pore space, but its particles have rigid characteristics that can effectively inhibit the influence of the compaction of particles and adjacent areas (Wang et al., 2017). Simultaneously, large-scale pyrite will induce the formation of microcracks and maintain a moderate opening, while irregular granular pyrite is more cemented between clay mineral flakes. Effective support is formed to prevent intergranular pores from becoming completely compacted, allowing for the filling and storage of liquid hydrocarbons (Li, 2022). Furthermore, the organic pores formed by liquid hydrocarbon cracking can be effectively preserved due to pyrite's "pillared" protection. In general, the earlier the pyrite cementation is formed, the higher the degree of development and the more conducive to mechanical compaction, formation, and preservation of organic pores in the later stage (Wang et al., 2019; Lu et al., 2022).

There have been few successes in analyzing the sedimentary environment of pyrite in the Longmaxi Formation shale in the upper Yangtze region. Although many researchers have made clear the impact relations between the two in terms of the indicative significance of pyrite on shale gas energy storage, there is no significant amount of theoretical data support. The present research defines the origin of pyrite, restores the shale sedimentary environment, and analyzes the impact of pyrite formation on the evolution of organic matter and the transformation of reservoir properties, providing a reference for the prediction of organic shale reservoirs through a comprehensive analysis of the structure, content, and particle size of pyrite in the shale of the Longmaxi Formation.

2 GEOLOGICAL SETTING

The Sichuan Basin is an essential part of the upper Yangtze plate and the most promising area for oil and gas exploration in southern China. The Changning main anticline structure is situated at the intersection of the Sichuan Basin and the Yunnan Guizhou Plateau, between the low and steep structural area of the ancient depression middle uplift in the South Sichuan and the Loushan fold belt (**Figure 1A**) (Chen et al., 2014; Huang et al., 2018).

The Longmaxi Formation of Silurian is the main target interval for shale gas exploration in the study area. The black shale of the Longmaxi Formation is in integrated contact with the black siliceous and calcareous shale of the Upper Ordovician Wufeng Formation, containing the Hirnantia–Dalmanitina fauna. The Longmaxi Formation has a thickness of 0 m 373 m, and it can be further subdivided into two lithologic sections: the first member of the Longmaxi Formation (S_1L_1) and the second member of the Longmaxi Formation (S_1L_2) (Zhu et al., 2018).

The rhythmic boundary is found between the gray–black shale at the bottom of the second member of the S_1L_2 formation and the black shale gray silty shale in the overlying S_1L_1 member. According to the secondary cycles and lithologic characteristics, it can be divided into two subsegments from the bottom ($S_1L_1^1$ and $S_1L_1^2$). The lithologic interface is the dark gray shale at the bottom of the $S_1L_1^2$ member and the gray-black shale of the underlying $S_1L_1^1$ member.

The $S_1L_1^1$ sub-member is a set of black carbonaceous shale rich in organic matter. Many graptolite groups with different shapes

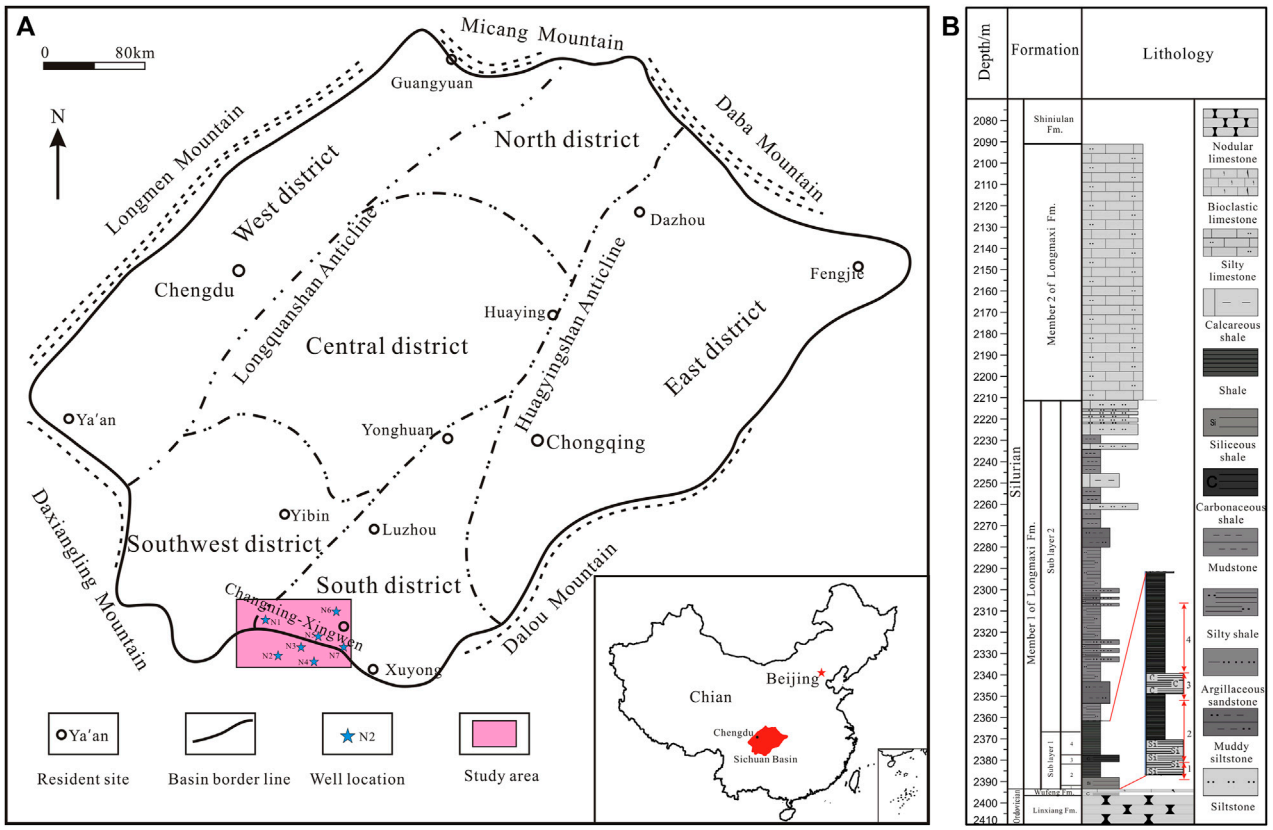

FIGURE 1 | (A) Location of the study area in the Sichuan Basin (Modified from Chen et al. (2014)); **(B)** stratigrapy of the Longmaxi Formation in well N3.

are developed, belonging to the calcareous outer shelf facies. It can also be subdivided into four sub-layers ($S_1 L_1^{1-1}$, $S_1 L_1^{1-2}$, $S_1 L_1^{1-3}$, and $S_1 L_1^{1-4}$) (**Figure 1B**).

3 METHODS

The data of Longmaxi Formation conventional logging, elemental capture spectroscopy (ECS), XRD (whole rock analysis), and porosity of seven wells were collected systematically. Mineral and pore structure characteristics, XRD (whole rock minerals), and total organic carbon (TOC) tests were carried out on 80 core samples from 7 wells.

Quanta 450 ESEM was used to examine the minerals and pore characteristics of shale samples. The pores in the SEM images were extracted and measured using PerGeos software from the FEI.

XRD analysis was performed using the PANalytical X'Pert PRO. The particle sizes of the shale powder were measured at less than 200 mesh.

The TOC content was measured using a LECO CS230 carbon/sulfur analyzer according to the national standard GB/T 19145–2003 after the samples were crushed into small particles of less than 0.2 mm in size and were treated with hydrochloric acid to remove the carbonates at 60–80°C.

The pyrite particle size and pore diameter of the shale sample were measured using Corephic v2.1 measurement software. More than 100 pyrite particle size data were collected for each shale sample. The sedimentary environment characteristics of pyrite formation were studied using the maximum particle size method (MFD) (Wignall et al., 2005), box-and-whisker plot (Wignall et al., 2005), and binary graphic method after data collection (Wilkin et al., 1996). The box-and-whisker plot can intuitively reflect the variation of lithology along with the depth, maximum and minimum particle sizes of framboidal pyrite, the middle particle size, and the distribution characteristics of particle concentration or dispersion (Wilkin et al., 1996; Wei et al., 2016; Wignall et al., 2016). The binary diagram of average particle size, standard deviation, and skewness also serves as potential methods for analyzing the redox conditions of sedimentary water (Wilkin et al., 1996; Chang et al., 2009).

4 RESULTS

4.1 Morphology and Particle Size Characteristics of Pyrite

SEM image shows that pyrite in the Longmaxi Formation of the study area is well developed and distributed in shale in different forms.

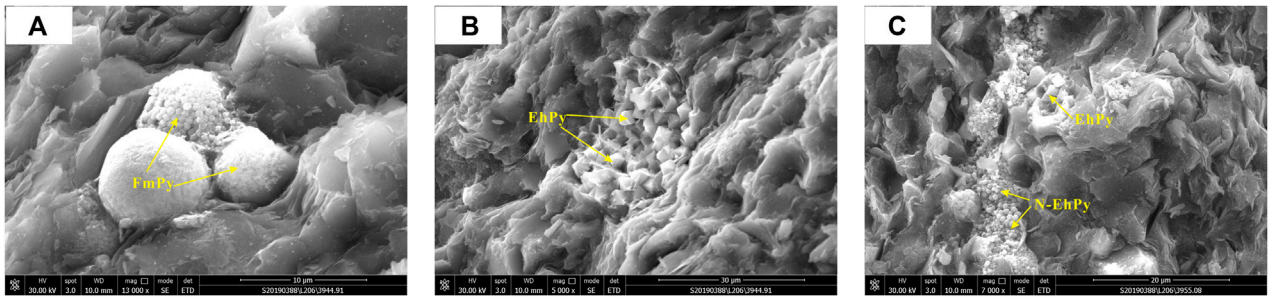

FIGURE 2 | Photomicographs of authigenic pyrite morphologies. **(A)** SEM image of typical framboidal pyrite of the Longmaxi Formation, **(B)** SEM image of euhedral pyrite of the Longmaxi Formation **(C)**. SEM image of banded shape and non-euhedral pyrite of the Longmaxi Formation.

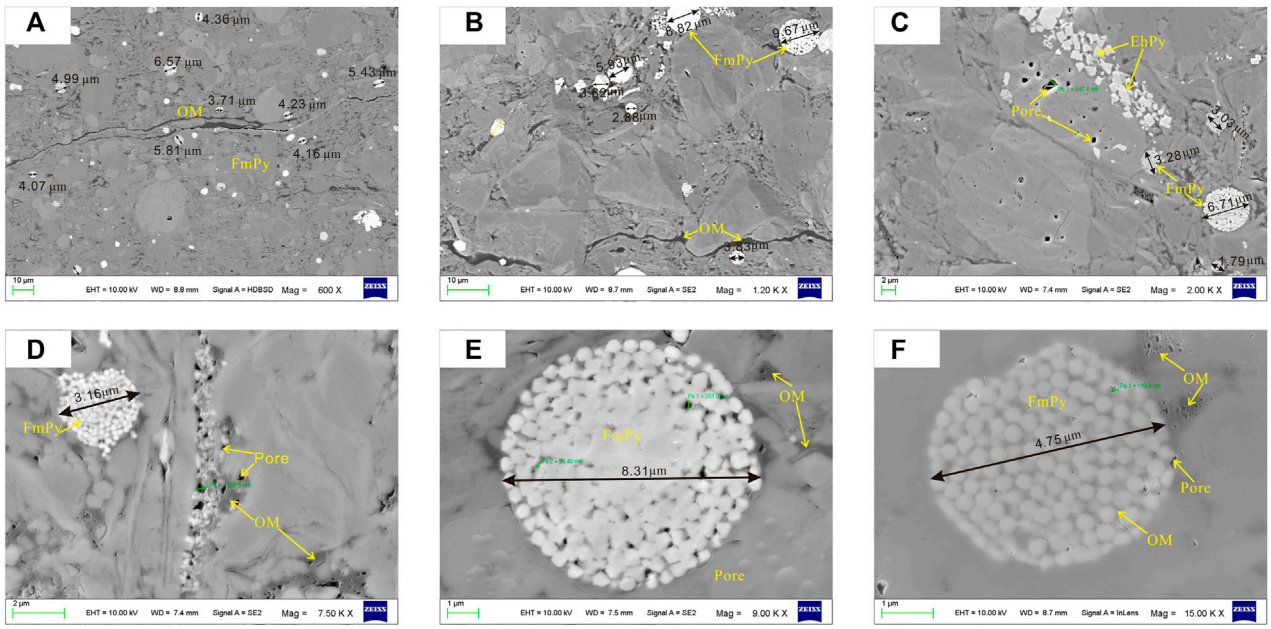

FIGURE 3 | Measurement of framboidal pyrite diameters *via* Corephic v2.1 software. Pyrite from samples of the Longmaxi Formation. OM = organic matter; FmPy = framboidal pyrite; Ehpy = euhedral pyrite.

Aggregating multiple granular microcrystals form framboidal pyrite in the form of spheres and sub spheres (**Figure 2A**). The diameter of a single crystal is generally 0.1–1 μm; most of the pyrite structures are well preserved, with a small number of pyrite microcrystals having secondary growth. The morphology of microcrystals changes from spherical to euhedral irregular shapes. A few framboidal pyrites recrystallize and lose their framboid structure. This is the most common type of pyrite in the study area.

The crystal structure of euhedral pyrite is octahedral, cubic, and spherical. It typically manifests as isolated crystals and aggregates (**Figure 2B**). It is frequently euhedral or semi-euhedral crystals with significant variation in the particle size. In general, euhedral pyrite aggregates form near organic matter and framboidal pyrite aggregates or marginal gaps.

Banded pyrite, which belongs to non-euhedral pyrite, is slender banded with an obvious directional arrangement and is mainly distributed at the junction of organic matter, mineral particles, and intergranular pores (**Figure 2C**).

Pyrite is primarily found in areas where organic matter is abundant. It is distributed in a long strip along the direction of organic matter development or concentrated in areas where organic matter and clay minerals coexist. Pyrite will form in small amounts near inorganic minerals or between mineral particles and in mineral particles.

The test characteristics of particle size of pyrite in shale show that the particle size distribution of framboidal pyrite in $S_1L_1^2$ members is 2.077–6.045 μm, with an average of 4.34 μm, 1.027–10.277 μm in $S_1L_1^1$ member, with an average of 4.31 μm. The particle size of $S_1L_1^{1-2}$ and $S_1L_1^{1-3}$ in the lower part is larger than that of pyrite in the shale at the top and bottom layers. In the deep Wufeng Formation, the particle size distribution of pyrite is 1.424–12.97 μm, with an average value

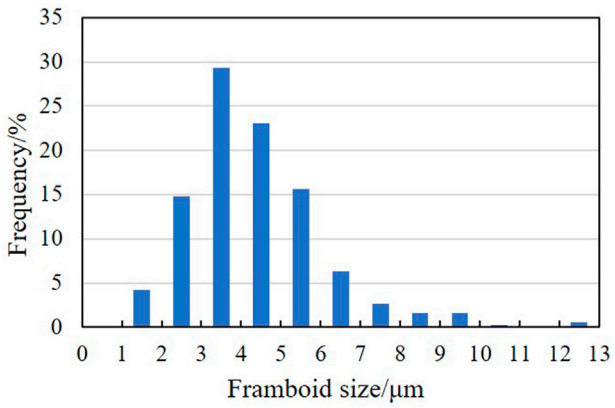

FIGURE 4 | Pyrite framboid size distribution histogram.

of 4.4 μm (**Figure 3**). In general, the particle size of framboidal pyrite is a single peak distributed from 1 to 13 μm, with a peak value of 3–5 μm (**Figure 4**). The particle size of pyrite increases first and then decreases from bottom to top, with the peak value of particle size distribution in the $S_1L_1^{1-2}$ (**Table.1**).

4.2 Vertical Distribution Characteristics of Pyrite and TOC

Considering N1 wells as an example, the vertical distribution characteristics and depth changes of pyrite, S element, and TOC are drawn (**Figure 5**).

The vertical variation of the pyrite content is more evident than that of the particle size. The pyrite content is distributed from 0.3 to 7.9%, with an average of 2.31%. Among them, the average content of Wufeng formation is 0.6%, the content of $S_1L_1^2$ is 0.8–7.9%, with an average of 1.8%; and the content of $S_1L_1^1$ is 1–5.9%, with an average of 3.0% The content of $S_1L_1^{1-2}$ and $S_1L_1^{1-3}$ layer sections is the highest, with average values of 2.6 and 3.9%, respectively; the content of pyrite increased first and then decreased.

The TOC of shale in the Longmaxi Formation is 0.23–4.93%, with an average of 1.78%. ECS logging data show that the content of the S element in the Longmaxi Formation is 0.001 kg/kg to 0.03 kg/kg, with an average of 0.01 kg/kg. Overall, TOC and S values show a positive correlation trend. After a sharp increase from the Wufeng formation to the bottom of the Longmaxi Formation, these two parameters maintain high values in $S_1L_1^1$. According to the fitting between the logging curve and the test TOC results, the predicted TOC value ranges from 2.8 to 6.7%, with an average value of 3.75%. Notably, higher TOC corresponds to higher porosity. In this interval, the average porosity of shale is greater than 4.8% and can reach up to 6.28%, indicating good reservoir capacity.

The vertical characteristics of TOC and S values indicate that the bottom of the Longmaxi Formation lies in an occluded reduction environment, whereas the top lies in an oxygen-deficient/reduction environment. The TOC content has strong compliance with the S element. The changing trend is basically the same, reflecting the dependence of organic matter enrichment in shale on sulfide sedimentary environment, which is closely related to the S element. The more reductive the sedimentary environment is, the more conducive it is to enriching organic matter (Wu C. et al., 2014; Han and Li, 2019).

TABLE 1 | Pyrite framboid size distributions *via* SEM images and Corephic v2.1 software measurement. SD = standard deviation; MFD = maximum framboid diameter; SK = skewness.

Samples	SD (μm)	Min (μm)	Mean (μm)	MFD (μm)	SK
$S_1L_1^2$	2.246	2.077	4.34	6.045	2.322
$S_1L_1^{1-4}$	1.374	1.027	2.51	4.043	0.696
$S_1L_1^{1-4}$	1.226	1.403	3.43	5.495	0.133
$S_1L_1^{1-3}$	1.824	1.235	4.31	9.738	1.094
$S_1L_1^{1-3}$	1.463	1.514	4.14	8.974	0.971
$S_1L_1^{1-2}$	1.553	2.027	4.79	9.745	0.635
$S_1L_1^{1-2}$	2.513	2.514	5.15	10.277	1.275
$S_1L_1^{1-1}$	1.196	1.852	3.66	5.879	0.205
Wufeng Formation	3.890	1.424	4.69	12.97	2.000
Wufeng Formation	1.406	2.493	4.35	9.924	1.904

5 DISCUSSION

5.1 Formation Environment of Pyrite

Framboidal pyrite can retain its original shape and size after burial; thus, it is frequently used to indicate the redox conditions of the water environment in modern marine sediments (Wilkin et al., 1996). Pyrite is the most commonly found near the chemical alteration layer. When the bottom water body is euxinic, pyrite is rapidly deposited on the sediment surface after formation, with large quantities and a small variation range of particle sizes. Under reduction conditions, pyrite with small particle sizes and a large amount will form near the interface between the sediment and water body in an environment with a lack of H_2S and oxygen, dominated by framboidal pyrite (Wignall and Newton, 1998; Bond and Wignall, 2010; Zhou et al., 2017). Pyrite grows in the pore water between oxygen-poor sediment particles below the sedimentary interface in the oxygen and oxygen-poor environment. The oxidant in the sediment is gradually consumed due to bacterial sulfate reduction. Once the sulfide environment is formed, framboidal pyrite is formed; Fe^{2+}, H_2S, and elemental sulfur are continuously and slowly supplied, resulting in a long growth time and a slow growth rate of pyrite; framboidal and euhedral pyrite will then appear with large and different sizes (Wilkin et al., 1996,1997). With increasing oxidation degree, larger particle size euhedral pyrite can form at the interface between the sediment and water, whereas oxidation produces only a small amount of euhedral pyrite (Wignall and Newton, 1998; Bond and Wignall, 2010).

The final formation of pyrite is controlled by the local microenvironment (Chang et al., 2020), and the process results from the combined influence of several factors (Berner, 1984). 1) Sulfate reduction and pyrite burial rates are significantly positively correlated with organic carbon burial rates (Lin et al., 2000). Therefore, the content and activity of organic matter become the primary factors limiting the formation of

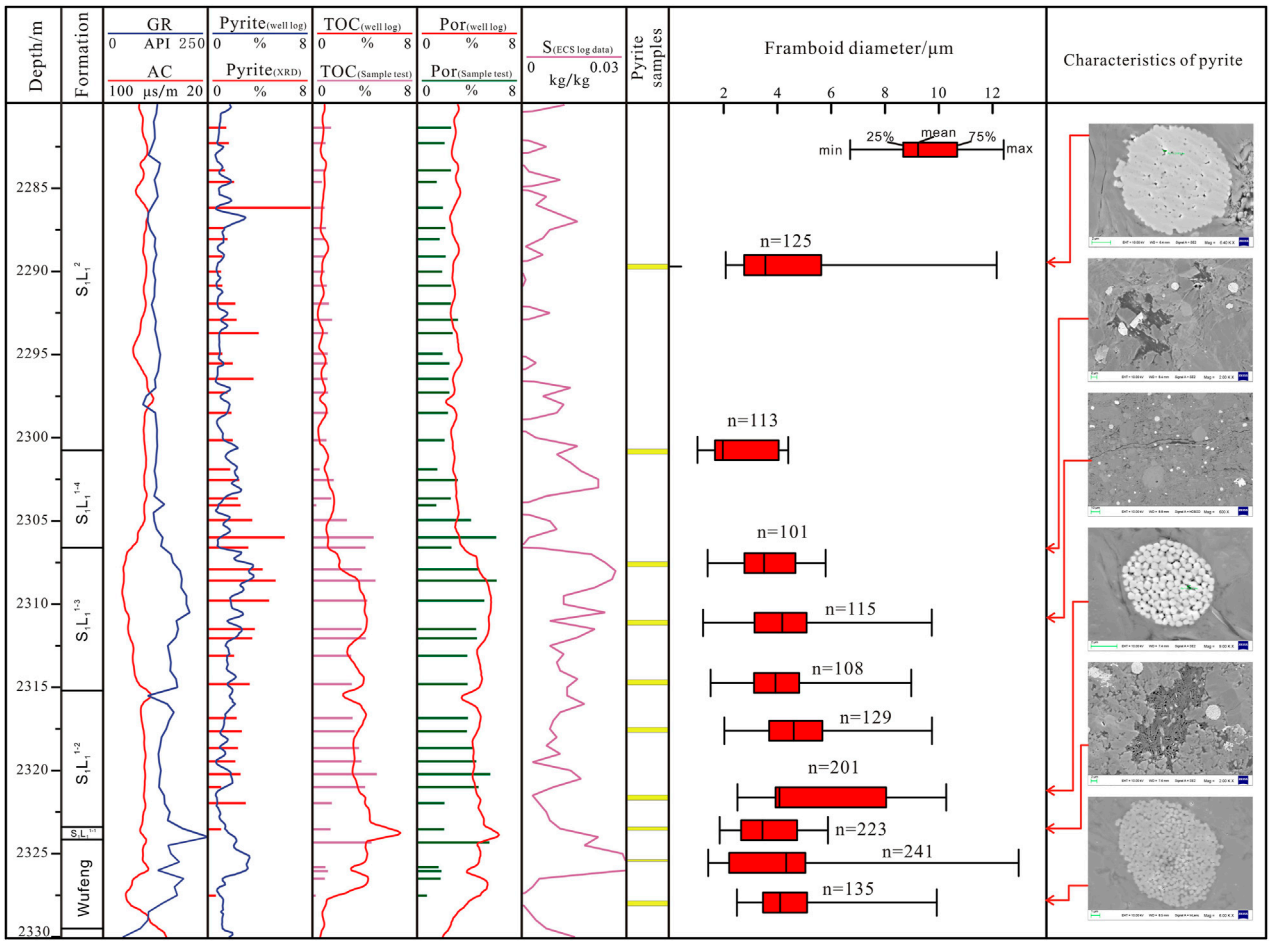

FIGURE 5 | Comprehensive comparison of geochemistry, reservoir physical properties and pyrite distribution characteristics of shale in the Longmaxi Formation.

authigenic pyrite. Terrestrial organic matter is relatively difficult to decompose and is not conducive to sulfate reduction reaction. 2) The diagenetic system gradually transits from open to closed with an increased water depth. The sulfate content in pore water is gradually consumed and limited, controlling the formation and burial of authigenic pyrite (Gomes and Hurtgen, 2013). According to the vertical variation of the sulfate content, soluble sulfur, and pyrite sulfur isotope signal in pore water, the formation of pyrite can be divided into four stages: 1) rapid reduction of sulfate, acid-soluble volatile sulfur yield is higher than that of pyrite; 2) the sulfate reduction rate and the yield of acid-soluble volatile sulfur began to decrease, and pyrite formed slowly; 3) sulfate content began to decrease, indicating the formation of the closed environment; 4) if organic carbon remains after sulfate is exhausted, authigenic pyrite enriched with ^{34}S will continue to be generated with SO_4^{2-} in the adjacent horizon (Chang et al., 2020). The closed diagenetic environment is conducive to the formation of pyrite; 3) in the redox sequence, organic carbon is buried and utilized by methanogens to generate CH_4, which diffuses upward in the sulfate methane transition zone, causing intense microbial sulfate reduction activity, leading to the enrichment of pyrite and the decomposition of natural gas hydrate (Zhang and Wu, 2019); 4) the deposition rate affects the formation of pyrite by changing other limiting factors. A high deposition rate is accompanied by the high organic matter content. However, when the deposition rate is too high, it will dilute the organic matter in the sediment (Tyson, 2001), reduce the residence time of sulfide at the redox interface, and lead to the incomplete conversion of acid-soluble volatile sulfur to pyrite (Chang et al., 2020).

Wilkin et al. (1996) proposed restoring the sedimentary environment using the box-and-whisker diagram of framboidal pyrite. The diagram in **Figure 3** shows the median, average, distribution range, and quartile of the particle size, which can intuitively reflect the distribution characteristics of maximum and minimum particle sizes, intermediate particle size, and particle concentration or dispersion of framboidal pyrite with depth (Wei et al., 2016; Wignall et al., 2016). The binary diagram of average particle size, standard deviation, and skewness can also be used to assess deposition redox conditions (Wilkin et al., 1996; Chang et al., 2009).

The oxygen and hydrogen sulfide concentrations in modern marine water can be divided into four categories: oxic, suboxic, anoxic, and euxinic (Tribovillard et al., 2006). The parameter

TABLE 2 | Characteristics of framboids used to define oxygen-related depositional conditions and facies (Bond and Wignall, 2010).

Conditions	Framboid parameters
Euxinic (persistently sulfidic lower water column)	Small (mean 3–5 μm), abundant, with narrow size range. Framboids dominate pyrite fraction
Anoxic (no oxygen in bottom waters for long periods)	Small (mean 4–6 μm), abundant, with a few, larger framboids. Framboids dominate pyrite fraction
Lower dysoxic (weakly oxygenated bottom waters)	Mean 6–10 μm, moderately common, with a few, larger framboids and some crystalline pyrite
Upper dysoxic (partial oxygen restriction in bottom waters)	Moderately common to rare, broad range of sizes, only a small proportion <5 μm. Majority of pyrite as crystals
Oxic (no oxygen restriction)	No framboids, rare pyrite crystals

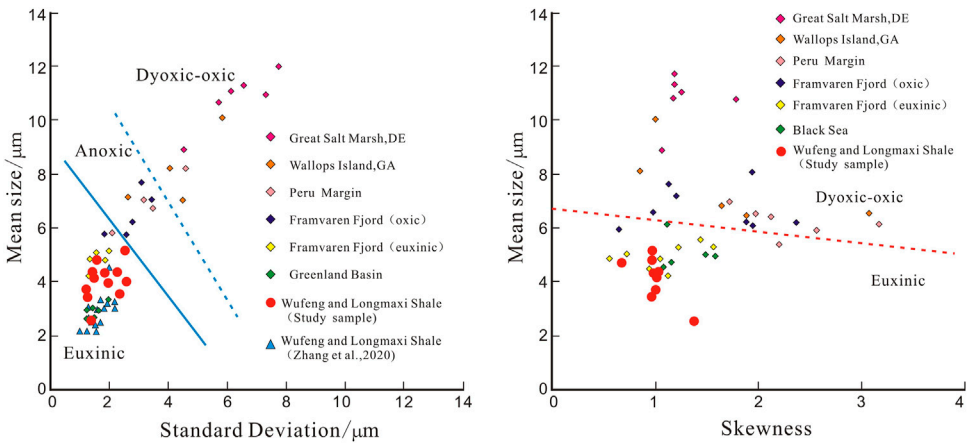

FIGURE 6 | Plot of the mean vs. the standard deviation (after Zhou et al., 2017; Zhang et al., 2020) and the mean vs. the skewness of the framboid size distribution (after Zhou et al., 2017).

characteristics of framboidal pyrite under different redox conditions are proposed (**Table.2**), which can be widely applied to the restoration of paleoenvironmental conditions in the sediments of various strata. The particle size distribution range of framboidal pyrite is narrow in the closed water environment (euxinic), but it tends to widen as the oxygen content increases.

The average particle size and skewness of framboidal pyrite can also identify the redox conditions for sediment formation (**Figure 6**) (Wilkin et al., 1996; Wei et al., 2016). Skewness is a good indicator of the heterogeneity of particle size distribution. When the variation range of framboidal pyrite particle size is small, it indicates a closed or semi-closed environment (**Figure 6**) (Wilkin et al., 1996).

The average particle size and standard deviation of the samples in this study are compared with the previous data. The sedimentary environment of Longmaxi formation samples in the study area is a euxinic environment (**Table.1**). Combined with the data in **Figure 6**, it can be inferred that the shale sedimentary environment of the Longmaxi Formation is the euxinic environment, which has strong reducibility, poor water fluidity, and a closed state. Pyrite cannot grow fully due to rapid settlement and burial after crystallization, resulting in generally small particle size characteristics due to an insufficient supply of materials, reducing agents, and energy required during the grain growth period of pyrite under poor hydrodynamic conditions. However, this closed euxinic environment with low long-term hydrodynamic force boosts organic matter deposition, accumulation, and preservation in Longmaxi Formation shale (Han and Li, 2019).

In sedimentation, shale is comprehensively controlled by the basin structure, water environment, sediment supply, and other factors, forming lithofacies that can reflect different environmental characteristics. According to the mineral composition, the shale in the study area can be divided into three lithofacies types: siliceous shale, calcareous shale, and mixed shale facies (Wang et al., 2016). The content and type of pyrite in different lithofacies are significantly different. The bottom of the Longmaxi Formation is dominated by siliceous shale, and mixed shale is occasionally seen. The development of banded pyrite and intermittent sandy lamina in the shale indicates a relatively quiet deep-water reduction environment in the sedimentary period, with the most pyrite content (Sun et al., 2019). The lithofacies in the middle and lower part of Longmaxi changed from siliceous shale to mixed shale, with scattered pyrite and relatively developed silty laminae, reflecting that the sedimentary environment changed from an early strong reduction environment to a weak reduction environment and decreased the pyrite content. Siliceous shale and mixed shale are more conducive to pyrite formation than calcareous shale (Lu et al., 2021).

5.2 Genetic Mechanism of Pyrite

Sedimentary pyrite is formed by reducing Fe^{3+} ions in sediments to Fe^{2+} ions in a strong reduction environment. Fe^{2+} ions react

with a large amount of H_2S produced by bacteria that decompose organic matter or sulfate-reducing bacteria. Reducing sulfate in sediments to form hydrometeorite pyrite ($FeS{\cdot}nH_2O$) or monosulfide iron, hydrometeorite pyrite reacts with elemental sulfur to form colloidal pyrite ($FeS_2{\cdot}nH_2O$), colloidal pyrite crystallizes and dehydrates to form pyrite (FeS_2) (Zhu and Geng, 2002).

Pyrite can be formed in two cases. The first is that it can be formed and precipitated directly from the solution under low in-situ active iron concentration. The second is to form mackinawite, greigite, framboidal pyrite, and euhedral pyrite under the high solubility of in-situ active iron. The formation stage of pyrite can be divided into the sedimentary and diagenetic types (Liu et al., 2016).

Sedimentary pyrite was formed in the synsedimentary period and early diagenetic stage. Sulfate-reducing bacteria reduce sulfate ions in the reducing water environment to produce H_2S or HS^-. Sulfide reacts with active iron Fe^{2+} to form tetragonal pyrite Fe_9S_8. (Bontognali et al., 2008; Heywood et al.,1990) Tetragonal pyrite is further transformed into pyrite Fe_3S_4. Pyrite particles are then aggregated under the influence of magnetic force to form framboidal pyrite (Wilkin et al., 1996).

$$2\,(CH_2O) + SO_4^{2-} \rightarrow 2HCO^{3-} + HS^-$$
$$CH_4 + SO_4^{2-} \rightarrow HS^- + HCO^{3-} + H_2O$$
$$S^{2-} + Fe^{2+} \rightarrow FeS_2$$

Diagenetic pyrite is formed in the stage of deep burial. In closed water with insufficient material supply (Wang, 2013), the concentration of active iron is low. Affected by the difference in pH value, pyrite can be formed either by crystallization directly from the water body or by forming FES first and then by some series of reactions (Cao and Wei, 2015). If the material supply and growth space are sufficient, framboidal pyrite with a large particle size will be formed. In contrast, self-shaped pyrite with small particles will be formed (Liu et al., 2016).

$$SO_4^{2-} + 1.33\,(CH_2) + 2H^+ \rightarrow H_2S + 1.33CO_2 + 1.33H_2O$$
$$S^{2+} + Fe^{2+} \rightarrow FeS_2$$

There is a small amount of lamellar and nodular pyrite in the Longmaxi Formation. At the formation stage, sediments are relatively loose, the supply of sulfur and iron is sufficient, and the pyrite microcrystals formed in the pores will gradually grow and increase until they fill the pore space. Following diagnoses such as compaction, pressure dissolution, and cementation, pyrite microcrystals in the space continue to grow and aggregate in the pores to form lumpy pyrite, which eventually forms euhedral, laminar, and nodular pyrites. This pyrite indicates the acidic sulfide reduction environment, which is conducive to the preservation and enrichment of organic matter.

The framboidal pyrite with the highest content in the Longmaxi formation is considered to have formed during a quasi syngenetic stage or early diagenesis in sedimentation (Marynowski and Zatoń, 2008). Barnes and Wilkin (1997). Framboidal pyrite is thought to have evolved through four continuous processes: 1) the formation of microcrystalline nuclei of ferrous sulfide, 2) the nucleation of colloidal pyrite (Fe_2S), 3) the gathering of colloidal pyrite crystallites to form a spherical strawberry body, and 4) the transformation of colloidal pyrite into framboidal pyrite (Cao and Wei, 2015; Zhou et al., 2017).

There has always been controversy about the organic or inorganic origin of pyrite. The view of biogenesis was put forward as early as 1923. Zhou and Jiang (2009) showed that framboidal pyrite is the illusion that cell aggregates or spherical organisms could be replaced by pyrite. Schouten (1946) once proposed that the framboidal structure has an inorganic origin. Yang and Gong (2011) opposed this inorganic origin of the biogenic view as framboidal pyrite was found in ores unrelated to the biological action (Lowenstam, 1981). In recent years, researchers have successfully synthesized strawberry pyrite in a vacuum anhydrous and aqueous solution. Sweeney believed that amorphous iron sulfide is formed in the initial stage of the reaction and then further reacts into equiaxed pyrite (Sweeney and Kaplan, 1973). Thus, the spherical structure is inherited when iron monosulfide is transformed into framboidal pyrite.

The authigenic pyrite in this sample has the general shape of a raspberry ball, and some balls develop octahedral microcrystals with very automorphic shapes. This is due to pyrite pellet nucleation, which crystallizes many microcrystals and transforms the pellets into raspberry balls. As a result, the formation of pyrite in the study area is more of inorganic nature. However, the genetic sequences, both organic-rich and organic-poor pyrites, could be established based on the degree of organic matter enrichment.

SEM images (**Figure 7**) depict the relationship between pyrite and organic matter, consistent with previous research: 1) organic matter is filled around or inside framboidal pyrite, indicating that its formation time is earlier than the kerogen massive oil generation period (Lu et al., 2021). 2) The aggregation of some framboidal pyrite microcrystals occurs in the space limited by the structure of organic matter. When pyrite grows to a certain extent, it is limited by organic matter and cannot continue to increase (MacLean et a1., 2008). 3) Euhedral pyrite aggregates often exist near the edge gaps of organic matter and framboidal pyrite aggregates.

The genetic sequence of organic-rich framboidal pyrite in the study area is established: 1) pyrite microcrystals nucleate and begin to aggregate and grow in the space limited by the structure of organic matter during the sulfate reduction stage of organic matter decomposition; 2) growing pyrites and microcrystals congregate to fill the remaining space in the cubic crystal form or the ubiquitous pentagonal dodecahedron. At the same time, it will cause many microspheres to form. These tiny pellets eventually evolved into euhedral pyrite crystals; 3) it extends and grows into framboidal pyrite through automorphic growth; 4) when there is little or no organic matter between the microcrystals in framboidal pyrite, the microcrystal particles fuse with each other under the condition of close aggregation so that the inclusions in the microcrystals and the organic matter mixed between the microcrystals disappear or are pushed out to form subhedral and subhedral shape pyrite crystals (**Figure 7**).

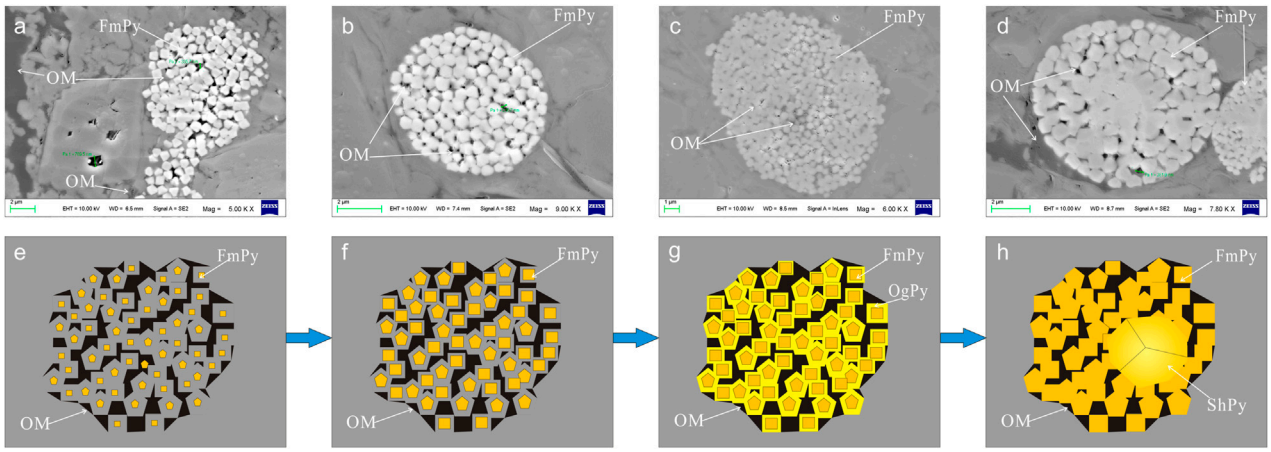

FIGURE 7 | Genetic model of framboidal pyrite in organic-rich shale. OM = organic matter; FmPy= framboidal pyrite; OgPy= pyrite overgrowth; ShPy = subhedral pyrite.

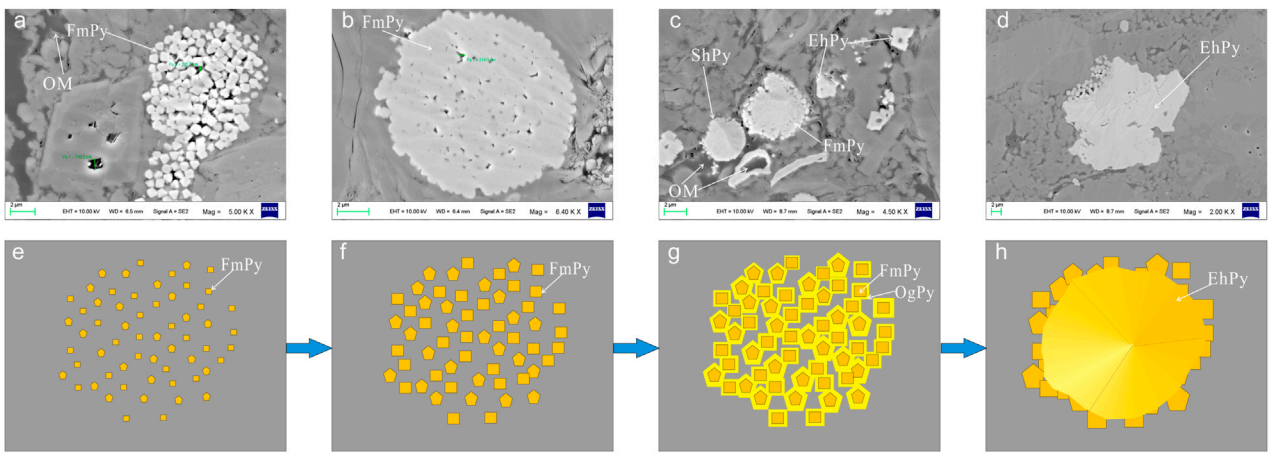

FIGURE 8 | Genetic model of framboidal pyrite in organic-poor shale. OM = organic matter; FmPy= framboidal pyrite; OgPy= pyrite overgrowth; EhPy= euhedral pyrite.

More experiments have confirmed the inorganic genesis of framboidal pyrite compared to the complex genesis affected by organic matter (Zuo et al., 2021). According to the microscopic characteristics, the inorganic genetic sequence is established: 1) the pyrite microcrystals continue to grow after nucleation, and the microcrystals increase and form cubic crystals or pentagonal dodecahedrons to gather and fill in the pore space; 2) after the microcrystal particles grow in their shape, they grow radially around the pyrite nodules to form raspberry pyrite; 3) due to the lack of organic matter and other substances, framboidal pyrite continues to grow and recrystallize, and finally fill the gap between single crystals to form self-shaped pyrite (**Figure 8**).

Notably, the saturation degree of the solution determines the crystal morphology of pyrite during the process of crystal growth. The appearance of self-shaped crystals indicates that the sulfur concentration in the sedimentary environment presents a long-term low saturation, and the sedimentary environment is conducive to the enrichment of organic matter.

5.3 Effect of Pyrite on Organic Matter

TOC (total organic carbon) is the total organic carbon in sediments (Canfield, 1994; Schoepfer et al., 2015). High marine primary productivity and reduced water environment are conducive to high TOC values in sediments. Pyrite generally exists in the shallow surface sediments of the continental margin sea. As the degradation product of organic matter and stable solid reduced sulfur, pyrite is preserved in the anoxic environment. The burial and decomposition conditions of organic matter in various sedimentary environments lead to significant differences in the contents of total organic carbon and pyrite sulfur (Wu L. et al., 2014).

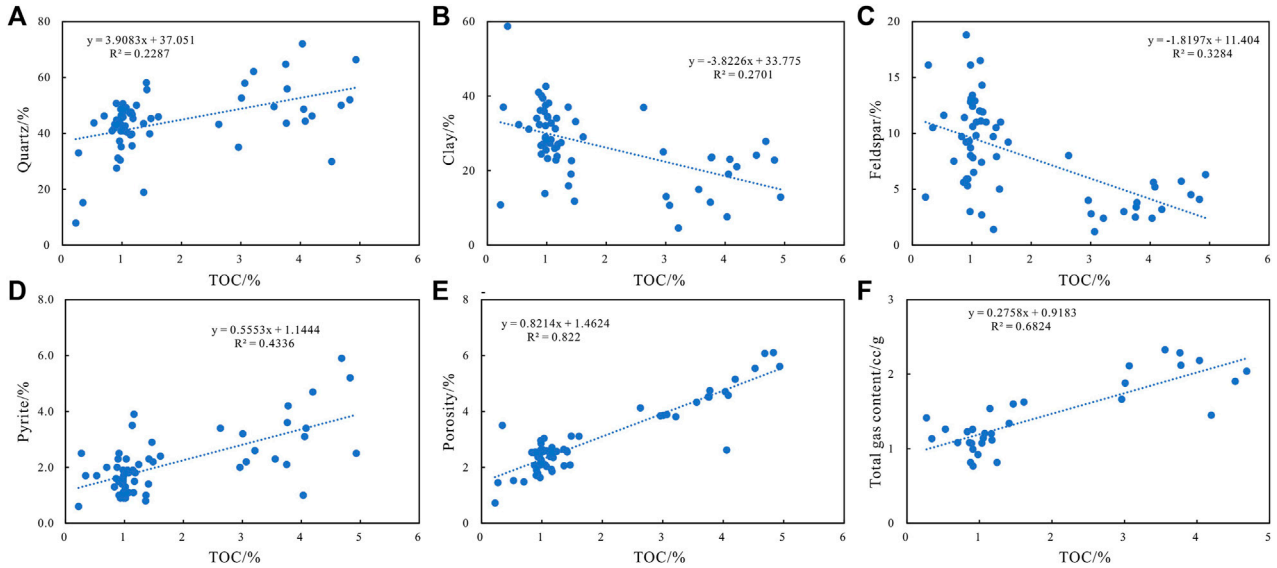

FIGURE 9 | Correlation diagram between TOC, shale mineral components, porosity, and total gas content. Quartz: quartz content, Clay: clay content, Feldspar: feldspar content, Pyrite: pyrite content of the shale samples.

Cao et al. (2018) proposed that the sedimentary environment restricts the type of organic matter and pyrite, and they are closely related. Organic matter provides a reductant and energy source during the formation of pyrite (Li et al., 2018). The organic parent material biofilm provides a necessary chemical environment for the structure and growth of pyrite. After sulfate-reducing bacteria degrade the initial organic matter, the generated H_2S reacts with iron to form pyrite (Wacey et al., 2015). Sulfur-rich kerogen takes a relatively lower time to generate hydrocarbon, and its C–S bond energy is lower, making it easier to decompose and generate hydrocarbon. In marine shale, sulfur mainly exists in the form of pyrite (Huang et al., 2017), and the formation of pyrite can reduce the activation energy of kerogen reaction and catalyze the hydrocarbon generation of organic matter (Zhang and Zhang, 1996). During diagenesis and diagenetic evolution, pyrite can weaken the compaction effect on organic matter and protect and support organic matter pores (Sun and Guo, 2017).

The sulfide reduction environment for the enrichment of framboidal pyrite is conducive to the enrichment and preservation of organic matter. The higher the iron content in water, the more conducive to the generation and enrichment of organic matter (Zhang et al., 2020). In the same sedimentary stage, the concentration of active iron and sulfur ions in the sedimentary environment controls the formation of pyrite. Framboidal pyrite positively correlates with the shale organic matter content and adsorbed gas content (Shu, 2015). Therefore, pyrite can indicate the enrichment of organic matter in shale. In the burial diagenetic stage, framboidal pyrite is formed in the sulfide reduction environment. The higher the pyrite content, the stronger the seawater reduction environment, and the shallower the redox interface. This is more conducive to organic matter enrichment, consistent with the positive correlation between synsedimentary pyrite and TOC (Li et al., 2018). The enrichment of pyrite also reflects the excellent water reduction environment in the sedimentary period, conducive to the enrichment and preservation of organic matter.

Generally, the content of organic matter is high, and the mineralization degree of pyrite is also high. If the organic matter is insufficient, the formed FeS remains at a particular stage of monosulfide. In order to convert FeS to FeS_2, there must be an oxidant. Experimental research shows that elemental sulfur is the only possible oxidant causing this transformation.

$$3\,FeS + S \rightarrow Fe_3S_4$$
$$Fe_3S_4 + 2S \rightarrow 3FeS_2$$

Quartz in shale can also form a siliceous support framework, providing a good space for kerogen preservation. Inorganic minerals such as clay minerals also have a specific catalytic effect on kerogen (**Figures 9A–C**). Under the reduction condition of pyrite development, shale has a high TOC value, leading to a high degree of pore development and the total gas content of shale (**Figure 9F**). In the study area, the Longmaxi Formation is in a reducing sedimentary environment with rapid material exchange; thus, there is an apparent positive correlation between organic carbon in shale and sulfur content in pyrite that is significantly stronger than that of quartz, clay, and feldspar (**Figure 9**). However, the TOC content is not the highest in some samples, but there is an abnormally high pyrite content. The unusually high abundance of pyrite is difficult to explain by the causes of organic matter, so the correlation between the two is not absolute.

5.4 Effect of Pyrite on the Porosity of Shale Reservoir

The reservoir space types of organic-rich shale mainly include fractures, inorganic pores, and organic pores, among which the pores related to pyrite include organic pores and inorganic pores.

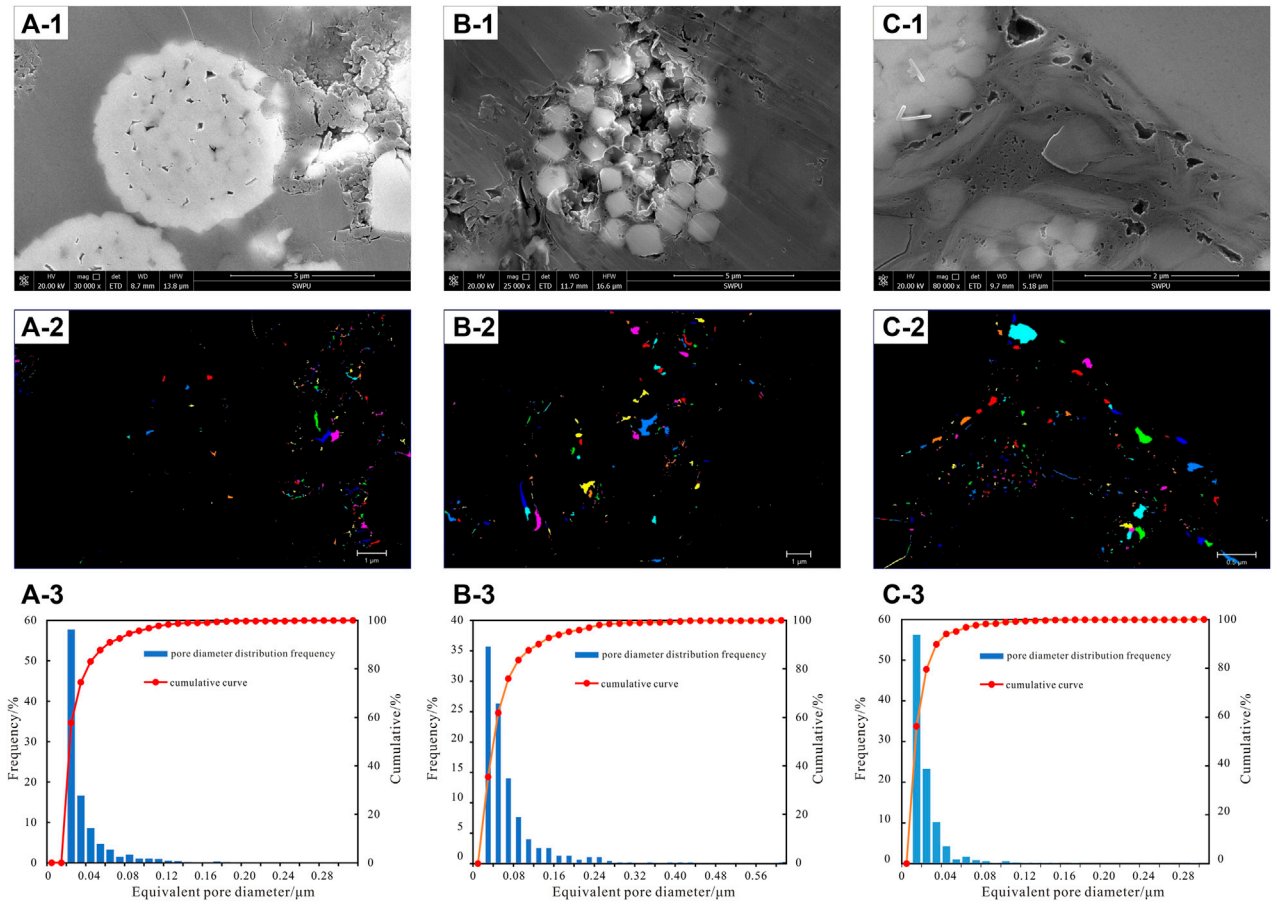

FIGURE 10 | Comparison of the pore structure characteristics of shale related to pyrite, (a-1, b-1, c-1 microscopic characteristics of shale, a-2, b-2, c-1 pore extraction characteristics, and a-3, b-3, c-3 equivalent pore diameter distribution), **(A)** 2326.45 m, well N2; **(B)** 2405.25 m, well N3; **(C)** 2215.36 m, well N4.

The inorganic pores are mainly the pores between the microcrystals of framboidal pyrite aggregate poor in organic matter and the mold pores formed by crystals falling off on the surface of the aggregate. In the former, the pores are often small, mostly isolated, and the pore diameter ranges from 0.02 to 0.04 μm due to the lack of restrictions on the radial growth of pyrite (**Figure 10**). The shape of the latter depends on the shape of the falling-off crystal, which is mostly honeycomb. The mold hole has good connectivity with the hole of organic matter in the crystal, and the pore diameter is large, which is the prominent enrichment place of free gas (Han and Li, 2019).

According to the relationship between pyrite and organic matter, organic pores can be divided into organic matter pores filling the interior of pyrite particles and organic matter pores between framboidal pyrite particles. The organic matter that fills the spaces between the grains of framboidal pyrite has mostly irregular pore morphology (Cao et al., 2018). Pyrite intergranular pores and organic matter pores are developed due to the limitation of organic matter. Intergranular pyrite pores will not expand after growing to a certain extent, and these pores are mainly organic matter pores, with the pore sizes ranging from 0.02 to 0.08 μm. The growth of pyrite affects the organic matter between pyrite particles, and the pore size of organic matter preserved under reduction conditions is generally 0.02–0.04 μm

There are numerous intergranular pores in framboidal pyrite and pores formed by pyrite intergranular filling organic matter, which provide storage space for gas accumulation. However, the influence of pyrite on the two types of pores differs. During the reservoir diagenesis process, the skeleton structure formed by stacking raspberry pyrite microcrystals can protect the development of nanopores between microcrystals by forming a “triangular stress protection structure” for the inorganic pores between pyrite grains (Zhao et al., 2018). The pores developed inside the organic matter contained in pyrite microcrystals. Pyrite aggregation protects the development of organic matter (Liu et al., 2017) and promotes the hydrocarbon generation and gas generation of organic matter by catalysis (Zhang and Zhang, 1996). Compared to shale without pyrite, the number of pores in pyrite is greater than that of the surrounding organic matter, and the number and size of organic pores in pyrite-enriched shale are larger.

The area ratio of framboidal pyrite aggregate is between 1.5 and 3.2%, and the average value is 1.8%. The face rate of framboidal pyrite aggregate is 3.5 ~ 9.5%, with an average

value of 5.8%, which is higher than the average face rate of the shale matrix. Therefore, pyrite pores have a positive contribution to the reservoir pore system. The pore contribution parameters of framboidal pyrite are obtained using the pyrite area ratio, the average face rate of pyrite, and the average face rate of the matrix, with the parameters ranging from 0.5 to 8%. Framboidal pyrite aggregate positively contributes to the reservoir pore system, and the pore diameter is small, primarily adsorption pores. Organic matter pores with diameters ranging from 10 to 50 nm in the framboidal pyrite aggregate are the most developed, accounting for more than 90% of the pores.

6 CONCLUSION

Framboidal pyrite, euhedral pyrite, and banded shape pyrite are all formed in the Longmaxi Formation shale, with framboidal pyrite being the most developed. The average particle size distribution of framboidal pyrite in the $S_1L_1^1$ member of the main reservoir is 3–5 μm, with the characteristics of a sulfidic environment. The average particle size of pyrite in a few shales is 4–6 μm, and it is oxygen-deficient in an anaerobic environment. The particle size of the sample in the lower part of the Longmaxi formation is between 1 and 15 μm, and the maximum particle size (MFD) is less than 20 μm, according to the box-and-whistler method. It is associated with an occluded reduction environment.

Two genetic sequences of framboidal pyrite are established based on the enrichment degree of shale organic matter and its associated relationship with pyrite. The formation of organic matter between pyrite microcrystalline particles will limit the continuous growth of pyrite, resulting in semi-euhedral and euhedral pyrite.

The sedimentary environment restricts the type of organic matter and pyrite. The reductive sedimentary environment of the Longmaxi Formation is conducive to the enrichment of organic matter, where the TOC value ranges from 0.23 to 4.93%, with an average value of 1.78%. There is a strong positive correlation between the pyrite content and TOC value. The TOC value of $S_1L_1^{1-2}$ and $S_1L_1^{1-3}$ members with the strongest reducibility is the highest, with the degree of pore development and total gas content are the strongest.

The pores related to pyrite in shale are mainly inorganic pores between microcrystals of framboidal pyrite aggregate, mold pores formed by crystals falling off on the surface of pyrite aggregate, organic matter pores inside pyrite particles, and organic matter pores between framboidal pyrite particles, organic pores are the main reservoir space. Also, pores are the main body of reservoir space. The enrichment of pyrite promotes the development of organic pores, and the number of pores in pyrite exceeds that of surrounding organic matter.

DATA AVAILABILITY STATEMENT

The original contributions presented in the study are included in the article/Supplementary Material; further inquiries can be directed to the corresponding authors.

AUTHOR CONTRIBUTIONS

JH and MW contributed in writing, reviewing, and editing, data curation, and writing—original draft preparation; LY, XS, SZ, LC, SP, and FW contributed in data analysis, mineral analysis, and graphic drawing.

FUNDING

This study received support from the Science and Technology Cooperation Project of the CNPC-SWPU Innovation Alliance (2020CX020000), China Postdoctoral Science Foundation (2017M623059), General Project of Chongqing Natural Science Foundation (No. cstc2021jcyj-msxmX0897), the Major Scientific and Technological Project of Sichuan Province (2020YFSY0039), and the Opening Foundation of Key Laboratory of Shale Gas Exploration, Minisitry of Natural Resources (KLSGE-202102).

ACKNOWLEDGMENTS

The authors would like to thank the PetroChina Southwest Oil and Gasfield Company for providing shale samples and experimental data. They appreciate the reviewers' suggestions.

REFERENCES

Berner, R. A. (1984). Sedimentary Pyrite Formation: An Update. *Geochimica Cosmochimica Acta* 48 (4), 605–615. doi:10.1016/0016-7037(84)90089-9

Bond, D. P. G., and Wignall, P. B. (2010). Pyrite Framboid Study of Marine Permian-Triassic Boundary Sections: A Complex Anoxic Event and its Relationship to Contemporaneous Mass Extinction. *Geol. Soc. Am. Bull.* 122 (7-8), 1265–1279. doi:10.1130/B30042.1

Bontognali, T. R. R., Vasconcelos, C., Warthmann, R. J., Dupraz, C., Bernasconi, S. M., and McKenzie, J. A. (2008). Microbes Produce Nanobacteria-like Structures, Avoiding Cell Entombment. *Geol* 36 (8), 663–666. doi:10.1130/G24755A.1

Canfield, D. E. (1994). Factors Influencing Organic Carbon Preservation in Marine Sediments. *Chem. Geol.* 114 (3/4), 315–329. doi:10.1016/0009-2541(94)90061-2

Cao, F., and Wei, H. (2015). Two Causes for the Low Abundance of Framboidal Pyrite in the Permian in Enshi Area in Hubei Province. *J. East China Inst. Technol. Nat. Sci.* 38 (2), 158–166. doi:10.3969/j.issn.1674-3504.2015.02.004

Cao, T., Deng, M., Song, Z., Liu, G. -X., Huang, Y. -R., Andrew, S. H., et al. (2018). Study on the Effect of Pyrite on the Accumulation of Shale Oil and Gas. *Nat. Gas. Geosci.* 29 (3), 404–414. doi:10.11764/j.issn.1672-1926.2017.12.006

Chang, H., Chu, X., Feng, L., Huang, J., et al. (2009). Framboidal Pyrites in Cherts of the Laobao Formation, South China: Evidence for Anoxic Deep Ocean in the Terminal Ediacaran. *Acta Petrol. Sin.* 25 (4), 1001.

Chang, H., and Chu, X. (2011). Pyrite Framboids and Palaeo Ocean Redox Condition Reconstruction. *Adv. Earth Sci.* 26 (5), 475. doi:10.12017/dzkx.2017.016

Chang, X., Zhang, M., Gu, Y., Wang, H., Liu, X., et al. (2020). Formation Mechanism and Controlling Factors of Authigenic Pyrite in Mud Sediments

on the Shelf of the Yellow Sea and the East China Sea. *Adv. Earth Sci.* 35 (12), 1306–1320. doi:10.11867/j.issn.1001-8166.2020.105

Chen, S., Zhu, Y., Qin, Y., Wang, h., Liu, H., and Fang, J. (2014). Reservoir Evaluation of the Lower Silurian Longmaxi Formation Shale Gas in the Southern Sichuan Basin of china. *Mar. Petroleum Geol.* 57, 619–630. doi:10.1016/j.marpetgeo.2014.07.008

Cui, J., Zhu, R., and Wu, S. (2013). The Effect of Pyrite on the Accumulation of Organic Matter, Hydrocarbon Generation and Expulsion, and Accumulation of Oil in Shale. *Geol. Review.59(supplement)* 1, 783.

Fan, C., Li, H., Qin, Q., He, S., and Zhong, C. (2020). Geological Conditions and Exploration Potential of Shale Gas Reservoir in Wufeng and Longmaxi Formation of Southeastern Sichuan Basin, China. *J. Petroleum Sci. Eng.* 191, 107138. doi:10.1016/j.petrol.2020.107138

Gomes, M. L., and Hurtgen, M. T. (2013). Sulfur Isotope Systematics of a Euxinic, Low-Sulfate Lake: Evaluating the Importance of the Reservoir Effect in Modern and Ancient Oceans. *Geology* 41 (6), 663–666. doi:10.1130/G34187.1

Han, S., and Li, W. (2019). Study on the Genesis of Pyrite in the Longmaxi Formation Shale in the Upper Yangtze Area. *Nat. Gas. Geosci.* 30 (11), 1608–1618. doi:10.11764/j.issn.1672-1926.2019.11.010

Heywood, B. R., Bazylinski, D. A., Garratt-Reed, A., Mann, S., and Frankel, R. B. (1990). Controlled Biosynthesis of Greigite (Fe_3S_4) in Magnetotactic Bacteria. *Naturwissenschaften* 77 (11), 536–538. doi:10.1007/BF01139266

Huang, H., He, D., Li, Y., Li, J., and Zhang, L. (2018). Silurian Tectonic-Sedimentary Setting and Basin Evolution in the Sichuan Area, Southwest china: Implications for Palaeogeographic Reconstructions. *Mar. Petroleum Geol.* 92, 403–423. doi:10.1016/j.marpetgeo.2017.11.006

Huang, Y., Zhang, X., Xiong, T., and Zhang, T. (2017). Profiling of Relationship between Shale Organic Matter Enrichment Mechanism and Gas-Bearing Property-A Case Study of Well QQ No. 1. *Coal Geol. China* 29 (12), 5–11. doi:10.3969/j.issn.1674-1803.2017.12.02

Li, D., Ou, C. H., Ma, Z. G., Jin, P. P., Ren, Y. J., and Zhao, Y. F. (2018). Pyrite-shale Interaction in Shale Gas Enrichment and Development. *Geophys. Prospect. Petroleum* 57 (3), 332–343. doi:10.3969/j.issn.1000-1441.2018.03.002

Li, H., Qin, Q., Zhang, B., Ge, X., Hu, X., Fan, C., et al. (2020). Tectonic Fracture Formation and Distribution in Ultradeep Marine Carbonate Gas Reservoirs: A Case Study of the Maokou Formation in the Jiulongshan Gas Field, Sichuan Basin, Southwest China. *Energy fuels.* 34 (11), 14132–14146. doi:10.1021/acs.energyfuels.0c03327

Li, H. (2022). Research Progress on Evaluation Methods and Factors Influencing Shale Brittleness: A Review. *Energy Rep.* 8, 4344–4358. doi:10.1016/j.egyr.2022.03.120

Li, H., Tang, H., Qin, Q., Zhou, J., Qin, Z., Fan, C., et al. (2019). Characteristics, Formation Periods and Genetic Mechanisms of Tectonic Fractures in the Tight Gas Sandstones Reservoir: A Case Study of Xujiahe Formation in YB Area, Sichuan Basin, China. *J. Petroleum Sci. Eng.* 178, 723–735. doi:10.1016/j.petrol.2019.04.007

Lin, S., Huang, K.-M., and Chen, S.-K. (2000). Organic Carbon Deposition and its Control on Iron Sulfide Formation of the Southern East China Sea Continental Shelf Sediments. *Cont. Shelf Res.* 20, 619–635. doi:10.1016/S0278-4343(99)00088-6

Liu, J., Yang, H., Xu, K., Wang, Z., Liu, X., Cui, L., et al. (2022). Genetic Mechanism of Transfer Zones in Rift Basins: Insights from Geomechanical Models. *GSA Bull.* doi:10.1130/B36151.1

Liu, Z. B., Gao, B., Hu, Z. Q., Du, W., Nie, H. K., and Jiang, T. (2017). Reservoir Characteristics and Pores Formation and Evolution of High Maturated Organic Rich Shale: a Case Study of Lower Cambrian Jiumenchong Formation, Southern Guizhou Area. *Acta Pet. Sin.* 38 (12), 1381–1389. doi:10.7623/syxb201712005

Liu, Z., Zhang, J., Liu, Y., Yu, W., He, W., and Li, B. (2016). The Particle Size Characteristics of Pyrite in Western Hunan and Hubei Areas' Wufeng-Longmaxi Formation Shale. *Sci. Technol. Eng.* 16 (26), 8. doi:10.3969/j.issn.1671-1815.2016.26.005

Lowenstam, H. A. (1981). Minerals Formed by Organisms. *Science* 211, 1126–1131. doi:10.1126/science.7008198

Lu, L., Liu, W., and Wei, Z. (2022). Diagenesis of the Silurian Shale, Sichuan Basin: Focus on Pore Development and Preservation. *Acta Sedimentol. Sin.* 40 (1), 73–87. doi:10.14027/j.issn.1000-0550.2021.125

Lu, Z., Tang, X., Zhang, T., Yufang, W., Jiazhcng, Z., Qingqiang, M., et al. (2021). Existence and Geological Significance of Pyrite in the Organic-Rich Shale of Lower Cambrian Niutitang Formation in Upper Yangtze Region. *Pet. Geology&Experiment* 43 (4), 599–610. doi:10.11781/sysydz202104599

MacLean, L. C. W., Tyliszczak, T., Gilbert, P. U. P. A., Zhou, D., Pray, T. J., Onstott, T. C., et al. (2008). A High-Resolution Chemical and Structural Study of Framboidal Pyrite Formed within a Low-Temperature Bacterial Biofilm. *Geobiology* 6 (5), 471–480. doi:10.1111/j.1472-4669.2008.00174.x

Marynowski, L., and Zatoń, M. K. (2008). Early Diagenetic Conditions during Formation of the Callovian (Middle Jurassic) Carbonate Concretions from Lukow (Eastern Poland): Evidence from Organic Geochemistry, Pyrite Framboid Diameters and Petrographic Study. *njgpa* 247, 191–208. doi:10.1127/0077-7749/2008/0247-0191

Nie, H., and Zhang, J. (2012). Shale Gas Accumulation Conditions and Gas Content Calculation:A Case Study of Sichuan Basin and its Periphery in the Lower Paleozoic. *Acta Geol. Sin.* 86 (2), 349–361. doi:10.3969/j.issn.0001-5717.2012.02.013

Schoepfer, S. D., Shen, J., Wei, H., Tyson, R. V., Ingall, E., and Algeo, T. J. (2015). Total Organic Carbon, Organic Phosphorus, and Biogenic Barium Fluxes as Proxies for Paleomarine Productivity. *Earth-Science Rev.* 149, 23–52. doi:10.1016/j.earscirev.2014.08.017

Shu, L. (2015). Geological Significance and Controlling Factors of Nonhydrocarbon Fluid of Jiufotang Formation in Naiman Sag. *Lithol. Reserv.* 27 (3), 75–81. doi:10.3969/j.issn.1000-1441.2018.03.002

Sun, C., Nie, H., Liu, G., et al. (2019). Quartz Type and its Control on Shale Gas Enrichment and Production:a Case Study of the Wufeng-Longmaxi Formations in the Sichuan Basin and its Surrounding Areas, China. *Earth Sci.* 44 (11), 3692–3704. doi:10.3799/dqkx.2019.203

Sun, Y. S., and Guo, S. B. (2017). Characteristics of Microscopic Pores of Shale from Upper Sinian Doushantuo Formation in the Western of Hunan and Hubei, China and the Main Controlling Factors. *J. Earth Sci. Env.* 39 (1), 114–125. doi:10.3969/j.issn.0001-5717.2012.02.013

Sweeney, R. E., and Kaplan, I. R. (1973). Pyrite Framboid Formation; Laboratory Synthesis and Marine Sediments. *Econ. Geol.* 68 (5), 618–634. doi:10.2113/gsecongeo.68.5.618

Tribovillard, N., Algeo, T. J., Lyons, T., and Riboulleau, A. (2006). Trace Metals as Paleoredox and Paleoproductivity Proxies: an Update. *Chem. Geol.* 232 (1-2), 12–32. doi:10.1016/j.chemgeo.2006.02.012

Tyson, R. V. (2001). Sedimentation Rate, Dilution, Preservation and Total Organic Carbon: Some Results of a Modelling Study. *Org. Geochem.* 32, 333–339. doi:10.1016/S0146-6380(00)00161-3

Wacey, D., Kilburn, M. R., Saunders, M., Cliff, J. B., Kong, C., Liu, A. G., et al. (2015). Uncovering Framboidal Pyrite Biogenicity Using Nano-Scale CNorg Mapping. *Geology* 43 (1), 27–30. doi:10.1130/G36048.1

Wang, M., Tang, H., Tang, H., Liu, S., Zhang, L., Zeng, M., et al. (2019). Impact of Differential Densification on the Pore Structure of Tight Gas Sandstone: Evidence from the Permian Shihezi and Shanxi Formations, Eastern Sulige Gas Field, Ordos Basin, china. *Geofluids* 2019 (2), 1–25. doi:10.1155/2019/4754601

Wang, M., Tang, H., Zhao, F., Liu, S., Yang, Y., Zhang, L., et al. (2017). Controlling Factor Analysis and Prediction of the Quality of Tight Sandstone Reservoirs: a Case Study of the He8 Member in the Eastern Sulige Gas Field, Ordos Basin, china. *J. Nat. Gas Sci. Eng.* 46, 680–698. doi:10.1016/j.jngse.2017.08.033

Wang, P., Huang, Y., Wang, C., Feng, Z., and Huang, Q. (2013). Pyrite Morphology in the First Member of the Late Cretaceous Qingshankou Formation, Songliao Basin, Northeast China. *Palaeogeogr. Palaeoclimatol. Palaeoecol.* 385 (5), 125–136. doi:10.1016/j.palaeo.2012.09.027

Wang, Y., Wang, S., Dong, D., Li, X., Huang, J., Zhang, C., et al. (2016). Lithofacies Characterization of Longmaxi Formation of the Lower Silurian, Southern Sichuan. *Earth Sci. Front.* 23 (1), 119–133. doi:10.13745/j.esf.2016.01.011

Wei, H., Wei, X., Qiu, Z., Song, H., and Shi, G. (2016). Redox Conditions across the G-L Boundary in South China: Evidence from Pyrite Morphology and Sulfur Isotopic Compositions. *Chem. Geol.* 440, 1–14. doi:10.1016/j.chemgeo.2016.07.009

Wignall, P. B., Bond, D. P. G., Sun, Y., Grasby, S. E., Beauchamp, B., Joachimski, M. M., et al. (2016). Ultra-shallow-marine Anoxia in an Early Triassic Shallow-Marine Clastic Ramp (Spitsbergen) and the Suppression of Benthic Radiation. *Geol. Mag.* 153 (2), 316–331. doi:10.1017/S0016756815000588

Wignall, P. B., Newton, R., and Brookfield, M. E. (2005). Pyrite Framboid Evidence for Oxygen-Poor Deposition during the Permian-Triassic Crisis in Kashmir. *Palaeogeogr. Palaeoclimatol. Palaeoecol.* 216 (3-4), 183–188. doi:10.1016/j.palaeo.2004.10.009

Wignall, P. B., and Newton, R. (1998). Pyrite Framboid Diameter as a Measure of Oxygen Deficiency in Ancient Mudrocks. *Am. J. Sci.* 298 (7), 537–552. doi:10.2475/ajs.298.7.537

Wilkin, R. T., Arthur, M. A., and Dean, W. E. (1997). History of Water-Column Anoxia in the Black Sea Indicated by Pyrite Framboid Size Distributions. *Earth Planet. Sci. Lett.* 148 (3-4), 517–525. doi:10.1016/S0012-821X(97)00053-8

Wilkin, R. T., Barnes, H. L., and Brantley, S. L. (1996). The Size Distribution of Framboidal Pyrite in Modern Sediments: an Indicator of Redox Conditions. *Geochimica cosmochimica acta* 60 (20), 3897–3912. doi:10.1016/0016-7037(96)00209-8

Wilkin, R. T., and Barnes, H. L. (1997). Formation Processes of Framboidal Pyrite. *Geochimica Cosmochimica Acta* 61 (2), 323–339. doi:10.1016/S0016-7037(96)00320-1

Wu, C., Zhang, M., Ma, W., Liu, Y., Xiong, D., Sun, L., et al. (2014a). Organic Matter Characteristic and Sedimentary Environment of the Lower Cambrian Niutitang Shale in Southeastern Chongqing. *Nat. Gas. Geosci.* 25 (8), 1267–1274. doi:10.11764/j.issn.1672-1926.2014.08.1267

Wu, L., Lei, H. Y., Ou, W. J., and Han, C. (2014b). Distribution Characteristic and Crystal Form of Pyrite from the Sediment Cores on Northern South China Sea. *J. Appl. Oceanogr.* 33 (1), 21–28. doi:10.3969/J.ISSN.2095-4972.2014.01.003

Yang, X., and Gong, Y. (2011). Pyrite Framboid: Indicator of Environments and Life. Diqiu Kexue - Zhongguo Dizhi Daxue Xuebao. *Earth Sci. - J. China Univ. Geosciences* 36 (4), 643–658. doi:10.3799/dqkx.2011.066

Zhang, G. R., Nie, H. K., Tang, X., Du, W., Sun, C. X., and Chen, S. (2020). Pyrite Type and its Effect on Shale Gas Accumulation: a Case Study of Wufeng-Longmaxi Shale in Sichuan Basin and its Periphery. *Pet. Geology&Experiment* 42 (3), 459–466. doi:10.11781/sysydz202003459

Zhang, J., and Zhang, P. (1996). A Discussion of Pyrite Catalysis on the Hydrocarbon Generation Process. *Adv. Earth Sci.* 11 (3), 282–287. doi:10.3321/j.issn:1001-8166.1996.03.009

Zhang, Y., and Wu, Z. (2019). Sedimentary Organic Carbon Mineralization and its Contribution to the Marine Carbon Cycle in the Marginal Seas. *Adv. Earth Sci.* 34 (2), 202–209. doi:10.11867/j.issn.1001-8166.2019.02.0202

Zhao, D. F., Guo, Y. H., Zhu, Y. M., Wang, G., Liu, J., Chong, X., et al. (2018). Micropore Characteristics and Geological Significance of Pyrite in Shale Rocks of Longmaxi Formation. *Acta Sedimentol. Snica* 36 (5), 864–876. doi:10.14027/j.issn.1000-0550.2018.077

Zhou, C., and Jiang, S.-Y. (2009). Palaeoceanographic Redox Environments for the Lower Cambrian Hetang Formation in South China: Evidence from Pyrite Framboids, Redox Sensitive Trace Elements, and Sponge Biota Occurrence. *Palaeogeogr. Palaeoclimatol. Palaeoecol.* 271 (3-4), 279–286. doi:10.1016/j.palaeo.2008.10.024

Zhou, J., Qiu, Z., Wang, H., Lu, B., and Jiang, Z. (2017). Formation Mechanism of Pyrite Framboid and its Research Significance. *Chin. J. Geol.* 52 (1), 242–253. doi:10.12017/dzkx.2017.016

Zhu, D., Liu, Q., Zhou, B., Jin, Z., and Li, T. (2018). Sulfur Isotope of Pyrite Response to Redox Chemistry in Organic Matter-Enriched Shales and Implications for Components of Shale Gas. *Interpretation* 6 (4), SN71–SN83. doi:10.1190/int-2018-0023.1

Zhu, Y. H., and Geng, J. J. (2002). Analysis on Causes of Depositional Pyrite under Different Environment. *Hebei Coal* 1, 11–12. doi:10.3969/j.issn.1007-1083.2002.01.006

Zou, C., Dong, D., Yang, H., Wang, Y., Huang, J., Wang, S., et al. (2011). Conditions of Shale Gas Accumulation and Planning Practices in China. *Nat. Gas. Ind.* 31 (12), 26–39. doi:10.3787/j.issn.1000-0976.2011.12.005,

Zuo, Q., Xu, Y., Yu, B., Zhang, C., Zhang, Y., Hou, C., et al. (2021). NanoSIMS Sulfur Isotope Studies of Pyrite from the Early Paleozoic Marine Shale: Implications for the Sedimentary Environment. *Mar. Petroleum Geol.* 124, 104802. doi:10.1016/j.marpetgeo.2020.104802

Conflict of Interest: XS, SZ and LC were employed by the Shale Gas Research Institute of PetroChina Southwest Oil and Gasfield Company.

The remaining authors declare that the research was conducted in the absence of any commercial or financial relationships that could be construed as a potential conflict of interest.

Publisher's Note: All claims expressed in this article are solely those of the authors and do not necessarily represent those of their affiliated organizations, or those of the publisher, the editors, and the reviewers. Any product that may be evaluated in this article, or claim that may be made by its manufacturer, is not guaranteed or endorsed by the publisher.